

PROBING THE OCEAN SURFACE WITH MICROWAVE RADAR

A simple physical picture is presented to show how microwave radiation is scattered from a rough surface that evolves with time. In particular, a model is proposed for computing the electromagnetic field scattered from a moving tilted plane containing small-scale roughness. The properties of the ocean surface are then incorporated in this model to qualitatively explain the variation of measured Ku-band radar cross sections and Doppler spectra as a function of the phase of a long ocean-surface wave.

INTRODUCTION

Considerable interest in the physics underlying the scattering of microwave radiation from the ocean surface has been generated by rapid advances in ocean remote sensing with microwave radars during the past decade or so. Those advances have been triggered by the extremely rich and varied data set collected during the Seasat mission in 1978. Although the Seasat satellite was operational for only three months, much of the data are still being examined. Further, many of the features visible in the synthetic aperture radar (SAR) images collected by Seasat have not yet been adequately explained.¹

The Seasat radars (SAR, wind scatterometer, altimeter), as well as those carried by subsequent satellites, have been generally used to collect backscatter cross-sectional data. Because of the high satellite speed, the coherence of the backscattered field is dominated by platform motion, and subtle effects caused by the time evolution of the short-scale surface waves (which are responsible for the backscattered power) usually cannot be measured. It is possible, however, to measure those effects from fixed or slowly moving platforms, and much information about surface-wave physics can be obtained from such coherence measurements.² We may find, in fact, that the only practical method for instantaneously measuring the ocean-surface roughness spectrum, at least in the short-wave region, is by using microwave techniques.

Clearly, an understanding of how the evolution of the ocean surface affects the scattered electromagnetic field is essential for an assessment of the feasibility of obtaining quantitative oceanographic data from a remote-sensing platform. Developing such an understanding is difficult, not only because of the problems associated with computing the scattering from a random surface with a broad band of roughness scales, but also because of the complicated hydrodynamics sometimes needed to describe the motion of the surface. One can, however, make "reasonable" assumptions about the surface behavior and then use those assumptions in the scattering models to calculate the scattered fields and compare them with measurements. As I will show, it is possible to describe seemingly complicated features of the scattered

fields with relatively simple assumptions about the surface structure.

I begin this article by presenting a general description of rough-surface scattering, which shows how surface-wave motion can affect the backscattered electromagnetic field, primarily through a simple Doppler-shift mechanism. I will then proceed to the specific problem of scattering from the moving ocean surface and show a few examples and comparisons with data.

GENERAL DISCUSSION OF ROUGH-SURFACE SCATTERING

Given a plane-wave electromagnetic field of the form

$$\mathbf{B}_I = \mathbf{B}_0 \exp[i(\mathbf{k} \cdot \mathbf{r}_1 - \omega_0 t)] , \quad (1)$$

incident on a "smooth" perfectly conducting surface along the direction of \mathbf{k} , the field \mathbf{B}_S scattered in the direction $\boldsymbol{\kappa}$ is given by

$$\mathbf{B}_S(\mathbf{r}_0, t) = \frac{\mathbf{B}_0 i}{4\pi} \frac{q^2}{q_z} \frac{e^{i(kr_0 - \omega_0 t)}}{r_0} \times \int G(\mathbf{x}) \exp(i\mathbf{q} \cdot \mathbf{r}_1) d\mathbf{x} , \quad (2)$$

where

$|\mathbf{k}|$ ($= |\boldsymbol{\kappa}|$) is the radar wave number,
 $\mathbf{q} = \mathbf{k} - \boldsymbol{\kappa}$,
 $\omega_0 = c |\mathbf{k}|$ is the radian frequency of the radar
 $c =$ speed of light,
 $G(\mathbf{x})$ is a function that describes the radar footprint, and
 \mathbf{x} is a two-dimensional vector in the horizontal plane.*

*For all computations in this article, we assume that the ocean is a perfect conductor. This assumption simplifies the mathematics and does not change any of our general conclusions.

The three-dimensional vector \mathbf{r}_1 in Equation 2 gives the distance from the center of the radar footprint to an arbitrary point on the ocean surface where the height (above the mean level) is $\eta(\mathbf{x}, t)$. Explicitly,

$$\mathbf{r}_1 = \mathbf{x} + \eta(\mathbf{x}, t)\hat{\epsilon}_z, \quad (3)$$

where $\hat{\epsilon}_z$ is a unit vector in the vertical direction. The distance from the center of the radar footprint to the radar platform is r_0 . Equation 2 says that the scattered field is simply proportional to the sum of the phase shifts, $\exp(\mathbf{q} \cdot \mathbf{r}_1)$, associated with each point on the scattering surface weighted by the value of the antenna footprint at that point. This is the Kirchhoff expression for the scattered field, which is exact for smooth mirror-like surfaces, but does not give the correct polarization dependence for the scattered field when the surface contains roughness scales on the order of the radar wavelength. It has recently been shown, however, that this

$$\mathbf{B}_S(\mathbf{r}_0, t) = \frac{\mathbf{B}_0}{2\pi i} \frac{k^2}{\kappa_z} \frac{e^{i(kr_0 - \omega_0 t)}}{r_0} \int G(\mathbf{x}) \exp[-2i\kappa_H \cdot \mathbf{x} - 2i\kappa_z \eta_L(\mathbf{x}, t)] (1 - 2i\kappa_z \eta_S(\mathbf{x}, t)) d\mathbf{x}. \quad (8)$$

deficiency can be corrected in a straightforward manner.³ Further, we have found⁴ that Equation 2 actually contains the essential features (except for the proper polarization dependence) of the heuristic composite model, which has been used extensively to compute radar scattering from the ocean surface (see, for example, Ref. 5). We will therefore use Equation 2 to further our general discussion of rough-surface scattering. Later, a more complicated expression that we have used for comparisons with data will be briefly discussed.

Suppose now that the surface is moving with horizontal velocity \mathbf{V}_H . Such a velocity might be caused by tidal flow, for example. To compute the field scattered from the same region of this surface as in the case of the stationary surface, we must replace $\eta(\mathbf{x}, t)$ in Equation 3 with $\eta(\mathbf{x} - \mathbf{V}_H t, t)$, since the surface is moving through the radar footprint with velocity \mathbf{V}_H . If we further assume the special case of backscattering for which $\mathbf{k} = \kappa$ so that $\mathbf{q} = 2\kappa$, Equation 2 becomes

$$\mathbf{B}_S(\mathbf{r}_0, t) = \frac{\mathbf{B}_0}{2\pi i} \frac{k^2}{\kappa_z} \frac{e^{i(kr_0 - \omega_0 t)}}{r_0} \int G(\mathbf{x}) \exp[-2i\kappa_H \cdot \mathbf{x} - 2i\kappa_z \eta(\mathbf{x} - \mathbf{V}_H t, t)] d\mathbf{x}, \quad (4)$$

where κ_z and κ_H are the vertical and horizontal components of κ , respectively. If we change integration variables, Equation 4 can be rewritten as

$$\mathbf{B}_S(\mathbf{r}_0, t) = \frac{\mathbf{B}_0}{2\pi i} \frac{k^2}{\kappa_z} \frac{e^{i(kr_0 - (2\kappa \cdot \mathbf{V}_H + \omega_0)t)}}{r_0} \int G(\mathbf{x}) \exp[-2i\kappa_H \cdot \mathbf{x} - 2i\kappa_z \eta(\mathbf{x}, t)] d\mathbf{x}, \quad (5)$$

where we have assumed that $|\mathbf{V}_H t|$ is small compared with linear dimensions of the radar footprint.* The ef-

fect of the moving surface is seen in Equation 5 as the familiar Doppler shift,

$$\Delta\omega = 2\kappa \cdot \mathbf{V}_H. \quad (6)$$

One can show that Equation 4 will also result when the surface is stationary and the platform is moving with velocity $-\mathbf{V}_H$.

To proceed further, it is convenient to partition the surface height $\eta(\mathbf{x}, t)$ into long scales specified by $\eta_L(\mathbf{x}, t)$ and short scales specified by $\eta_S(\mathbf{x}, t)$, such that

$$\eta(\mathbf{x}, t) = \eta_L(\mathbf{x}, t) + \eta_S(\mathbf{x}, t), \quad (7)$$

with $2\kappa_z \eta_S(\mathbf{x}, t) \ll 1$. We may then expand the short-wave portion of the exponential term in Equation 5 to obtain (with $\mathbf{V}_H = 0$)

Note that $\eta_S(\mathbf{x}, t)$ appears linearly in Equation 8 while $\eta_L(\mathbf{x}, t)$ appears exponentially.

As a simple form for $\eta(\mathbf{x}, t)$, which can be evaluated analytically and also, as we shall see later, has some relevance to backscattering from the ocean, we assume that

$$\eta_L(\mathbf{x}, t) = \tan(\alpha)x + V_z t, \quad (9)$$

and

$$\eta_S(\mathbf{x}, t) = h_s \cos(Kx - \Omega t). \quad (10)$$

The long-scale surface is a plane whose height increases linearly along the x -axis with slope $\tan\alpha$ and is independent of y . The elevation of the entire plane is moving

*Since the correlation time for microwave fields backscattered from the ocean surface, even at low wind speeds, is on the order of a few tenths of a second or less, this is a reasonable assumption if the footprint size is on the order of 1 m or more and the current is on the order of 1 m/s or less.

along the z -axis with velocity V_z . The short-scale surface is sinusoidal with amplitude h_s , wave number K , and frequency Ω propagating along the x -axis. Figure 1 shows a plot of such a surface as a function of x as time increases.* If we chose a Gaussian radar footprint of the form

$$G(\mathbf{x}) = \exp\left(-2\frac{x^2 + y^2}{L^2}\right), \quad (11)$$

where L is a characteristic footprint dimension, then we can integrate Equation 8 with the surface defined above to obtain

$$\mathbf{B}_S(\mathbf{r}_0, t) = \frac{\mathbf{B}_0}{4i} \frac{L^2 k^2}{\kappa_z} \frac{e^{i[kr_0 - (2\mathbf{k}\cdot\mathbf{v} + \omega_0)t]}}{r_0} \left\{ \exp\left[-\frac{L^2 k^2}{2 \cos^2 \alpha} \sin^2(\theta_I - \alpha)\right] - i\kappa_z h_s \right. \\ \left. \times \left(\exp\left[-\frac{L^2}{8 \cos^2 \alpha} (2k \sin(\theta_I - \alpha) + K)^2\right] + \exp\left[-\frac{L^2}{8 \cos^2 \alpha} (2k \sin(\theta_I - \alpha) - K)^2\right] \right) \right\}, \quad (12)$$

where θ_I is the radar incidence angle, the radar is looking along the x -axis, and the Doppler velocity \mathbf{V} is given by

$$\mathbf{V} = \frac{\Omega}{K} \hat{\epsilon}_x + V_z \hat{\epsilon}_z. \quad (13)$$

The expression in Equation 12 for the field scattered by our hypothetical surface contains some interesting features. To examine these features, we note that backscattered power is proportional to $|\mathbf{B}_S(\mathbf{r}_0, t)|^2$; that is,

$$\text{Power} \propto \exp\left[-\frac{L^2 k^2}{\cos^2 \alpha} \sin^2(\theta_I - \alpha)\right] + \kappa_z^2 h_s^2 \left(\exp\left[-\frac{L^2}{8 \cos^2 \alpha} (2k \sin(\theta_I - \alpha) + K)^2\right] \right. \\ \left. + \exp\left[-\frac{L^2}{8 \cos^2 \alpha} (2k \sin(\theta_I - \alpha) - K)^2\right] \right)^2. \quad (14)$$

The first term in Equation 14, proportional to the square of the first term in braces in Equation 12, depends only on the long-scale portion of the surface and is maximum when the radar incidence angle θ_I equals the slope angle α of the long-scale surface. This term is the “specular” scattering contribution and is analogous to reflection from a mirror. It approaches $\delta(\theta_I - \alpha)$ as the footprint size L approaches ∞ .

The second term in Equation 14 depends on both the long- and short-scale portions of the surface and is maximized if

$$K = \pm 2k \sin(\theta_I - \alpha), \quad (15)$$

*The numerical values of the parameters used to generate the surface shown in Figure 1 are $\alpha = 5^\circ$, $V_z = 0.1$ m/s, $h_s = 0.5$ m, $K = 0.63$ m⁻¹, and $\Omega = 2.48$ s⁻¹ (see Eqs. 10 and 11). These values are convenient for illustrating the features of $\eta(\mathbf{x}, t)$, but have no other particular physical significance.

the so-called Bragg condition. Thus, for a radar of fixed wave number and incidence angle, the strongest contribution from this term will occur from surface roughness scales corresponding to twice the radar wave number projected onto the scattering (not the horizontal) surface. This scattering mechanism, sometimes called tilted-Bragg scattering, approaches $\delta[K \pm 2k \sin(\theta_I - \alpha)]$ as L approaches ∞ .

Finally, we see from Equation 13 that the Doppler velocity associated with the field scattered from $\eta(\mathbf{x}, t)$ has two components. The horizontal component is equal to the phase speed, Ω/K , of the short-scale surface; the vertical component is just the long-scale surface motion

V_z . In the following section, we will see that the simple example discussed above has much in common with the more complicated problem of scattering from the ocean surface.

SCATTERING FROM THE OCEAN SURFACE

To particularize our discussion of rough-surface scattering to the ocean surface, we must now introduce some details of the properties of that surface. As everyone who has looked at the ocean knows, its surface contains a

broad band of roughness scales ranging from tens (or even hundreds) of meters down to small ripples with wavelengths that can be even shorter than the wavelength

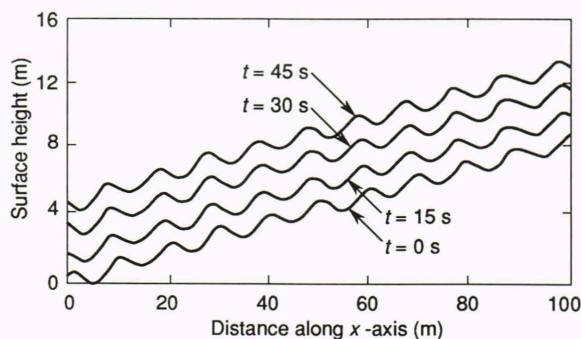


Figure 1. Sinusoid on tilted plane surface at 0, 15, 30, and 45 s (see Eqs. 10 and 11 and related discussion).

of a microwave radar. This broadband structure plays a crucial role in determining the nature of the backscattered electromagnetic field. In fact, one significant deficiency in current research on microwave remote sensing of the ocean is the lack of detailed knowledge of the shape of the ocean surface and its evolution. A statistical description of the surface is all that is generally available, and this is usually given in terms of a surface-wave spectrum $\psi(\mathbf{K})$ that is related to the autocovariance of the surface height by

$$\langle \eta(0,0)\eta(\mathbf{x},t) \rangle = \int \psi(\mathbf{K}) \cos(\mathbf{K} \cdot \mathbf{x} - \Omega t) d\mathbf{K}. \quad (16)$$

Here, Ω and K are related through the surface-wave dispersion relation

$$\Omega(\mathbf{K}) = \left\{ gK \left[1 + \left(\frac{K}{K_0} \right)^2 \right] \right\}^{1/2} + \mathbf{K} \cdot \mathbf{V}, \quad (17)$$

where g is the acceleration due to gravity, K_0 ($= 363 \text{ m}^{-1}$) is related to the surface tension of water, and \mathbf{V} is any additional background current such as we discussed above.

Most of our knowledge of $\psi(\mathbf{K})$ comes from point measurements of the wave-height frequency spectrum $\psi(\Omega)$ taken with a wire wave gauge or pressure sensor, for example. These measurements can then be converted to a K -spectrum using the dispersion relation of Equation 17 along with a critical assumption about the angular dependence of $\psi(\mathbf{K})$ as a function of K . Measurements of $\psi(\Omega)$ corresponding to waves of about 10 cm length or more can be made in the open ocean, whereas measurements for shorter waves are usually carried out in wave tanks. Several empirical models that parameterize these data in terms of the wind speed (or friction velocity) have been developed, and Figure 2 shows plots of $\psi(K)$ versus K for one such model, developed by Bjerkaas and Riedel,⁶ for wind speeds of 5, 10, and 15 m/s. Note that as the wind speed increases, the spectral peak also increases and moves to smaller K -values (longer waves)

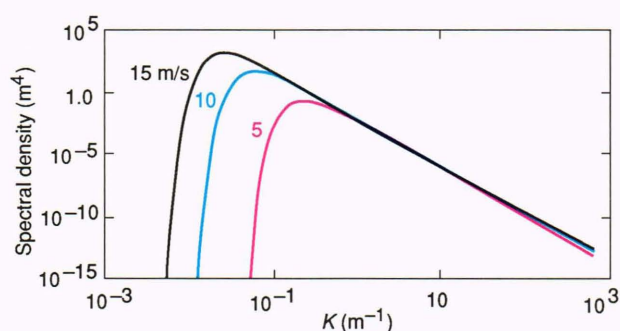


Figure 2. Wave-height spectrum versus K for wind speeds of 5, 10, and 15 m/s.

as expected, while the energy at K -values corresponding to 1 m or shorter waves ($K \geq 6 \text{ m}^{-1}$) remains generally constant with wind speed. In this so-called saturation region, $\psi(K)$ varies like K^{-4} . Note also that the surface-wave wave numbers in the saturation region coincide roughly with the electromagnetic wave numbers of microwave radars.

Using the properties of the height spectrum and the results of the simple scattering example discussed earlier, we can now begin to construct a qualitative picture of microwave backscattering from the ocean surface. A schematic of our hypothetical scattering experiment is shown in Figure 3. Again, most of the wave energy in the ocean surface is concentrated at the spectral peak, so we can consider the surface to be composed of a dominant wave with wavelength determined by the K -value at the peak. For a fully developed spectrum with a wind speed of 10 m/s, for example, the wavelength of such a wave is about 100 m. This dominant wave is represented by the sinusoidal surface in Figure 3. The shorter surface waves (in particular, the microwave-radar Bragg waves) are shown as sinusoids propagating over the surface of the dominant wave. Since we know from the form of the spectrum that these short waves have much less energy than the dominant wave, their amplitude is much smaller. As shown in Figure 3, all the waves are propagating in the wind direction (with phase speeds

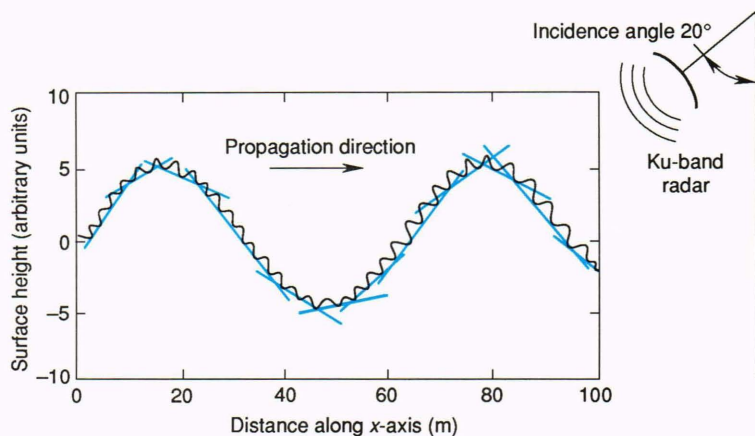


Figure 3. Qualitative representation of radar scattering from the ocean surface.

depending on K) toward the radar. If the radar footprint is small compared with the length of the dominant wave, then the portion of the long-wave surface sampled by the radar may be approximated by the tangent planes shown in the figure. The slope of these tangent planes depends on the phase of the dominant wave, and the maximum slope is only a few degrees, even at relatively high wind speeds. Further, these planes have a velocity component along a direction normal to their surface that depends on the orbital velocity of the dominant wave. The surface at each point on the front face of the wave moves up while each point on the back face moves down; as the planes move up and down, the small-scale waves of course move across them.

This picture recalls our simple example of short waves propagating on a plane. We now want to apply the results of that example to the present case, which is more relevant to ocean-surface scattering. Suppose we have a Ku-band radar (frequency, 14 GHz; wavelength, 2 cm) with a footprint of a few meters probing a surface such as that shown in Figure 3, looking into the wind at an incidence angle $\theta_i = 20^\circ$. What sort of backscattered power and Doppler velocity do we expect? On the basis of our previous example and the qualitative picture of the surface in Figure 3, we expect that the Doppler velocity should shift back and forth between plus and minus the orbital velocity of the dominant wave as the scattering surface in the radar footprint shifts between the front face and rear face of the long wave, respectively. This shifting is caused by the heaving motion of the long-wave surface discussed above. There should also be a mean Doppler velocity equal to the phase speed of the Ku-band Bragg waves. For the above geometry, this can be determined (from Eqs. 15 and 17) to be ≈ 0.25 m/s, corresponding to about an 8-Hz frequency shift. The Bragg wave number as defined by Equation 15 will decrease on the front face of the wave because the surface there is tilted toward the radar, and will increase on the back face because the surface tilts away. Since there is more power in the surface-wave spectrum at lower wave numbers, the backscattered power from the front face of the wave should, according to Equation 12, be greater than that from the back face. Thus, in our example the backscattered fields corresponding to the higher Doppler frequencies should have more power than those with lower Doppler shifts.

We have some experimental measurements corresponding closely to the situation just described,⁷ and we can use them to check the validity of our speculations. Specifically, we have about 20 minutes of complex Ku-band radar data collected from the Chesapeake Light Tower during the SAXON Experiment sponsored by the Office of Naval Research. These data were taken in ≈ 10 -m/s winds blowing almost directly toward the radar. We have determined the average frequency of each 1-s segment of the data, and we show in Figure 4 a histogram of the number of occurrences of each frequency. One sees from this figure that a significant fraction of the data has Doppler frequencies quite different from the 8-Hz Bragg frequency. This suggests that the motion of the long-wave surface plays an important role

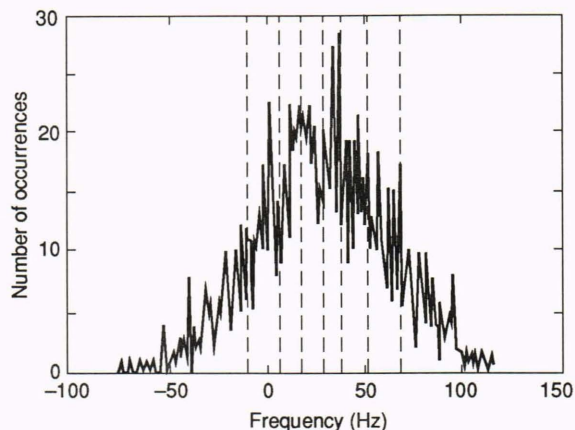


Figure 4. Histogram of 1-s average Doppler frequency.

in the scattering. We have partitioned the range spanned by Doppler frequencies in Figure 4 into eight bins, each containing an equal number of samples. The vertical dashed lines in the figure show the boundaries of these frequency bins. On the basis of our previous discussion, we interpret the field samples in these bins as having been scattered from a particular phase position on the long wave. The highest frequency bin, for example, contains samples of the field scattered from the phase position that has the largest velocity component toward the radar.

To continue, we look at the average autocovariance functions and Doppler spectra determined from the fields in each frequency bin in the histogram of Figure 4. The autocovariance of the backscattered field is given by

$$R(t) = \frac{4\pi r_0^2}{|\mathbf{B}_0|^2 A_{\text{eff}}} \langle \mathbf{B}^*(r_0, 0) \mathbf{B}(r_0, t) \rangle, \quad (18)$$

where A_{eff} is the effective footprint area, and we have normalized $R(t)$ so that $R(0)$ is the cross section per unit area. The Doppler spectrum is simply the Fourier transform of $R(t)$ and is given explicitly by

$$S(\omega) = \int_{-\infty}^{\infty} e^{-i\omega t} R(t) dt. \quad (19)$$

The peak position of the Doppler spectrum indicates the intrinsic frequency of the signal, and the area under the spectrum is the cross section per unit area. Using Equations 18 and 19, we have computed an average Doppler spectrum for each frequency bin in the histogram of Figure 4. (Since the autocovariance function $R(t)$ falls to zero in about 20 or 30 ms, the 1-s data samples used to generate the histogram are more than long enough for a meaningful Doppler estimate.) These eight spectra are shown in Figure 5. From the lowest to highest center frequency, they correspond to the lowest to highest frequency bins in the histogram of Figure 4, respectively. Note that the area under the spectra increases as the center frequency increases. This is in good agreement with our speculations, based on the simple model discussed

earlier, that the signals with the highest-frequency Doppler shifts should contain the most power. Thus, the largest spectrum in Figure 5, with center frequency of about 90 Hz, is representative of scattering from the front face of the long surface wave; the smallest spectrum, with center frequency of about -30 Hz, results from scattering from the conjugate phase position on the back face of the wave. The center frequencies of the largest and smallest spectra are not symmetric about zero frequency as one might expect, because there was also a mean surface drift toward the radar during the experiment (corresponding to the V_H term in Eq. 5), which, along with the motion of the Bragg scatters, causes the mean Doppler offset of about 25 Hz seen in Figure 5.

We see, then, that the Doppler frequency of the backscattered radar signal is a measure of the velocity of the ocean surface. Since we can relate this surface velocity to the surface height using Equations 16 and 17, we can, in principle, measure the surface-height spectrum $\psi(\mathbf{K})$ with the radar. The possibility of making such measurements has been recognized by Plant et al.² and was also confirmed using the Ku-band data discussed above. Further, since we know that surface waves obey the dispersion relation of Equation 17, we can also use Doppler measurements to discriminate surface-wave-induced motion from other motion sources. As discussed by Jensen elsewhere in this issue, Doppler measurements from a multifrequency delta-k radar have recently been used to measure the velocity of oceanic internal waves.

The comparisons with experimental data give us confidence that our ideas about how radar scatters from an evolving ocean surface are qualitatively correct. What is left now is to make quantitative comparisons with the available data. As stated earlier, the simple expression for the backscattered field given by Equation 8, although containing the essential features, does not correctly predict all the details of the backscattered field (e.g., polarization effects). Following the same basic approach as outlined above and in Ref. 4, we have developed a more precise expression for the scattered field that does include many of those details. (The derivation of this expression will not be given here, but the interested reader may refer to Ref. 8 and references contained therein.) It should be mentioned, however, that our expression does give the proper V-V and H-H polarization cross sections in the small-wave-height limit and also the proper (polarization-independent) specular scattering when no small-scale waves are present. The time dependence is included in this model by assuming linear evolution of the surface-wave spectrum, essentially using Equation 16. We have used this model to predict the dependence of Doppler spectra on such parameters as radar frequency, incidence angle, and look direction with respect to the wind.⁸ Further, applying concurrent *in situ* measurements of the long-wave spectrum as well as winds and mean surface currents, we have used it to make a quantitative prediction of the mean Doppler spectrum associated with the Ku-band radar data discussed above. A comparison of this prediction with the measured mean spectrum shows very good agreement (Ref. 7 and Thompson, Gotwols, and Keller, unpublished).

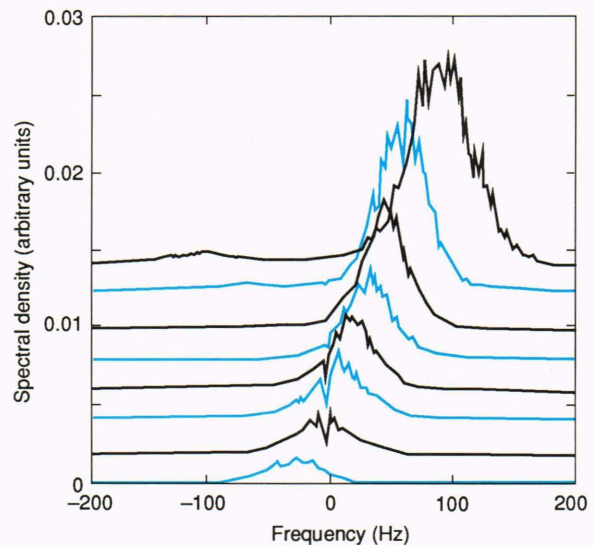


Figure 5. Average Doppler spectra at various locations along the long-wave phase.

CONCLUSION

One goal of this article has been to provide a physical picture of how microwave radiation is scattered from an evolving rough surface by considering the simple case of scattering from small-scale roughness on a moving plane. This picture motivated the development of a qualitative model for scattering from the ocean surface where a broad range of roughness scales exists. In particular, we have seen how the motion of the surface waves can affect the Doppler spectra of the radar return.

We have used our simple model to explain qualitatively the variation of measured Ku-band radar cross sections and Doppler spectra over the phase of a long ocean-surface wave. Detailed discussion of a more exact scattering model and its application to this problem may be found in Refs. 7 and 8. The goal of our work is to understand the surface-wave hydrodynamics and electromagnetic scattering processes well enough so that the inverse scattering can be solved; that is, to be able to use our knowledge of the radar return to extract information about the surface-height spectrum and its evolution.

Although much progress has been made over the last several years in understanding radar backscatter from the ocean, much work still remains. Accurate measurements of Doppler spectra are needed over the full range of incidence angles as a function of wind speed and direction as well as radar frequency. Concurrent direct measurements of the two-dimensional surface spectrum, if possible, would certainly enhance our ability to assess the scattering models and validate the assumptions made in their derivation. As these assessments progress, the operational use of microwave radar for measuring the properties of the ocean surface will become a definite possibility.

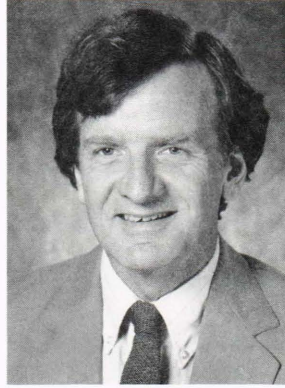
REFERENCES

- ¹Beal, R. C., DeLeonibus, P. S., and Katz, I., eds., *Spaceborne Synthetic Aperture Radar for Oceanography*, The Johns Hopkins University Press, Baltimore (1981).
- ²Plant, W. J., Keller, W. C., and Cross, A., "Parametric Dependence of Ocean Wave Radar Modulation Transfer Functions," *J. Geophys. Res.* **88**, 9747-9756 (1983).
- ³Holliday, D., "Resolution of a Controversy Surrounding the Kirchhoff Approach and the Small Perturbation Method in Rough Surface Scattering Theory," *IEEE Trans. Antennas Propag.* **35**, 120-122 (1987).
- ⁴Thompson, D. R., "Calculation of Radar Backscatter Modulations from Internal Waves," *J. Geophys. Res.* **93**, 12371-12380 (1988).
- ⁵Valenzuela, G. R., "Theories for the Interaction of Electromagnetic and Oceanic Waves—A Review," *Boundary Layer Meteorol.* **13**, 61-85 (1978).
- ⁶Bjerkaas, A. W., and Riedel, F. W., *Proposed Model for the Elevation Spectrum of a Wind-Roughened Sea Surface*, JHU/APL TG 1328 (1979).
- ⁷Thompson, D. R., Gotwols, B. L., Sterner, R. E., II, and Keller, W. C., "A Comparison of Ku-Band Doppler Measurements at 20° Incidence with Predictions from a Time-Dependent Composite Model," in *Proc. 1989 International Geoscience and Remote Sensing Symposium*, Vol. 3, p. 1921 (1989).
- ⁸Thompson, D. R., "Doppler Spectra from the Ocean Surface with a Time-Dependent Composite Model," in *Radar Scattering from Modulated Wind Waves*, Komen, G. J., and Oost, W. A., eds., Kluwer Academic Publishers, Dordrecht, pp. 27-40 (1989).

ACKNOWLEDGMENTS—It is a pleasure to acknowledge many useful discussions concerning the general topic of radar scattering from the ocean with

Bruce L. Gotwols and J. Robert Jensen at APL and with William C. Keller at the Naval Research Laboratory. I also thank Frank Herr at the Office of Naval Research for granting us access to the SAXON database.

THE AUTHOR



DONALD R. THOMPSON received a B.S. in physics from Case Western Reserve University in 1964 and a Ph.D. in physics from the University of Minnesota in 1968. After two years at the California Institute of Technology, Dr. Thompson returned to the University of Minnesota in 1970. From 1976 to 1978, he was an Alexander von Humboldt Foundation fellow at the Institute for Theoretical Physics at the University of Tübingen. Coming to APL in 1980, he has worked on the physics of ocean-surface waves and electromagnetic scattering theory in the Remote Sensing Group of the Submarine Technology Department. Since 1989, he has been with the Space Geophysics Group of the Space Department.